Supporting Information

Models for Unsymmetrical Active Sites in Metalloproteins: Structural, Redox, and Magnetic, Properties of Bimetallic Complexes with M^{II}–(μ-OH)–Fe^{III} Cores

Yohei Sano[†], Nathanael Lau[†], Andrew C. Weitz[‡], Joseph W. Ziller[†], Michael P. Hendrich*[,‡], A.S. Borovik*[,†]

[†]*Department of Chemistry, University of California – Irvine, 1102 Natural Sciences II, Irvine, CA 92697-2025, United States*

[‡]*Department of Chemistry, Carnegie Mellon University, Pittsburgh, PA 15213, United States*

E-mail: aborovik@uci.edu

Contents

Crystallography

General Methods. Single crystals were mounted on a glass fiber or loop and transferred to a Bruker SMART APEX II diffractometer. The APEX2[1] program package was used to determine the unit-cell parameters and for data collection. The raw frame data was processed using SAINT[2] and SADABS[3] to yield the reflection data file. Subsequent calculations were carried out using the SHELXTL[4] program. The structures were solved by direct methods and refined on F^2 by full-matrix least-squares techniques. The analytical scattering factors[5] for neutral atoms were used throughout the analyses. Hydrogen atom H(1) was located from a difference-Fourier map and refined (x,y,z and U_{iso}). The remaining hydrogen atoms were included using a riding model. In addition to the triflate counterion there were two molecules of dichloromethane solvent present. The molecular structures of [(TMTACN)M^{II}–(μ-OH)–Fe^{III}MST]OTf (M^{II} = Fe, Mn) have already been reported.[6]

Structure of [(TMTACN)Co^{II}–(μ-OH)–Fe^{III}MST]OTf. An orange crystal of approximate dimensions 0.106 x 0.253 x 0.280 mm was analyzed. The diffraction symmetry was mmm and the systematic absences were consistent with the triclinic space group *P*$\bar{1}$ that was later determined to be correct. Least-squares analysis yielded wR2 = 0.0709 and Goof = 1.037 for 738 variables refined against 12670 data (0.74Å), R1 = 0.0265 for those 11382 data with $I > 2.0\sigma(I)$.

Structure of [(TMTACN)Ni^{II}–(μ-OH)–Fe^{III}MST]OTf. An orange crystal of approximate dimensions 0.114 x 0.152 x 0.208 mm was analyzed. The diffraction symmetry was mmm and the systematic absences were consistent with the triclinic space group *P*$\bar{1}$ that was later determined to be correct. Least-squares analysis yielded wR2 = 0.1118 and Goof = 1.036 for 660 variables refined against 11911 data (0.77Å), R1 = 0.0426 for those 9209 data with $I > 2.0\sigma(I)$.

Structure of [(TMTACN)Cu^{II}–(μ-OH)–Fe^{III}MST]OTf. An orange crystal of approximate dimensions 0.156 x 0.376 x 0.426 mm was analyzed. The diffraction symmetry was mmm and the systematic absences were consistent with the orthorhombic space group *Pbca* that was later determined to be correct. Least-squares analysis yielded wR2 = 0.1947 and Goof = 1.217 for 719 variables refined against 11851 data (0.83Å), R1 = 0.0907 for those 9810 data with $I > 2.0\sigma(I)$.

Structure of [(TMTACN)Zn^{II}–(μ-OH)–Fe^{III}MST]OTf. An orange crystal of approximate dimensions 0.136 x 0.149 x 0.168 mm was analyzed. The diffraction symmetry was mmm and the systematic absences were consistent with the triclinic space group *P*$\bar{1}$ that was later determined to be correct. Least-squares analysis yielded wR2 = 0.1809 and Goof = 1.048 for 672 variables refined against 13151 data (0.75Å), R1 = 0.0660 for those 10084 data with $I > 2.0\sigma(I)$.

Table S1. Crystallographic data for [(TMTACN)M^{II}–(μ-OH)−Fe^{III}MST]$^+$ complexes (M^{II} = Co^{II}, Ni^{II}, Cu^{II}, Zn^{II}).

	[(TMTACN)Co^{II}–(μ-OH)–Fe^{III}MST]OTf	[(TMTACN)Ni^{II}–(μ-OH)–Fe^{III}MST]OTf	[(TMTACN)Cu^{II}–(μ-OH)–Fe^{III}MST]OTf	[(TMTACN)Zn^{II}–(μ-OH)–Fe^{III}MST]OTf
formula	$[C_{42}H_{67}CoFeN_7O_7S_3]$ $[CF_3SO_3]$ • (CH_3CN)	$[C_{42}H_{67Ni}FeN_7O_7S_3]$ $[CF_3SO_3]$ • (CH_3CN)	$[C_{42}H_{67}CuFeN_7\ O_7\ S_3]$ $[CF_3SO_3]$ • $3(CH_2Cl_2)$	$[C_{42}H_{67}ZnFeN_7O_7S_3]$ $[CF_3SO_3]$ • $1.5(CH_2Cl_2)$
fw	1183.11	1182.89	1401.44	1275.88
T (K)	88(2) K	88(2) K	143(2) K	88(2) K
crystal system	Triclinic	Triclinic	Orthorhombic	Triclinic
space group	$P\bar{1}$	$P\bar{1}$	*Pbca*	$P\bar{1}$
a (Å)	11.6341(5)	11.6180(16)	17.047(2)	11.8947(6)
b (Å)	15.6144(6)	15.620(2)	27.052(4)	15.7190(9)
c (Å)	15.7195(6)	15.659(2)	28.045(4)	15.8049(9)
α (°)	80.3235(4)	80.0664(18)	90	82.0438(7)
β (°)	69.3935(4)	69.2828(17)	90	88.8630(7)°.
γ (°)	89.8327(4)	89.7521(18)	90	70.7837(7)
Z	2	2	8	2
V (Å^3)	2629.97(18)	2613.1(6)	12933(3)	2762.5(3)
δ_{calc} (mg/m^3)	1.494	1.503	1.440	1.534
indep. reflections	12670	11911	11851	13151
R1	0.0265	0.0426	0.0907	0.0660
wR2	0.0709	0.1118	0.1947	0.1809
Goof	1.037	1.036	1.217	1.048
CCDC#	1571442	1571443	1571445	1571444

$wR2 = [\Sigma[w(F_o^2-F_c^2)^2] / \Sigma[w(F_o^2)^2]\ ]^{1/2}$

$R1 = \Sigma||F_o|-|F_c|| / \Sigma|F_o|$

$Goof = S = [\Sigma[w(F_o^2-F_c^2)^2] / (n-p)]^{1/2}$ where n is the number of reflections and p is the total number of parameters refined.

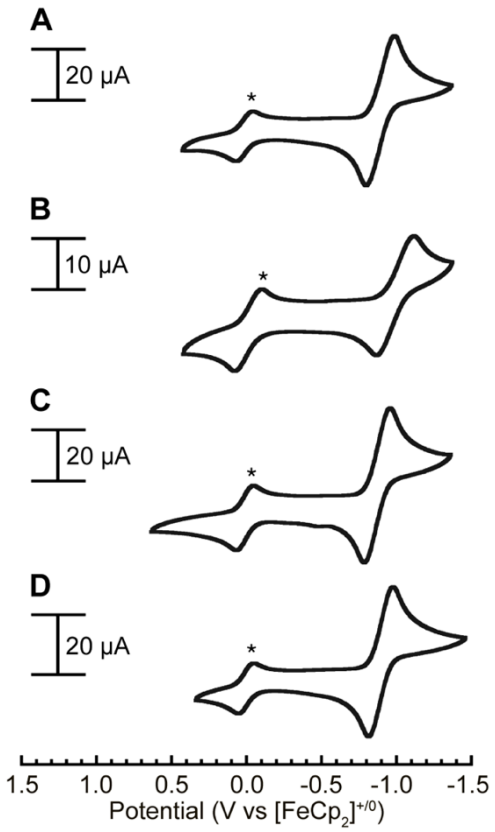

Figure S1. Cyclic voltammograms of (**A**) [(TMTACN)Co^{II}–(μ-OH)–Fe^{III}MST]$^+$, (**B**) [(TMTACN)Ni^{II}–(μ-OH)–Fe^{III}MST]$^+$, (**C**) [(TMTACN)Cu^{II}–(μ-OH)–Fe^{III}MST]$^+$, and (**D**) [(TMTACN)Zn^{II}–(μ-OH)–Fe^{III}MST]$^+$. The cyclic voltammograms were collected at 100 mV s^{-1} in the presence of [$FeCp_2$] (*).

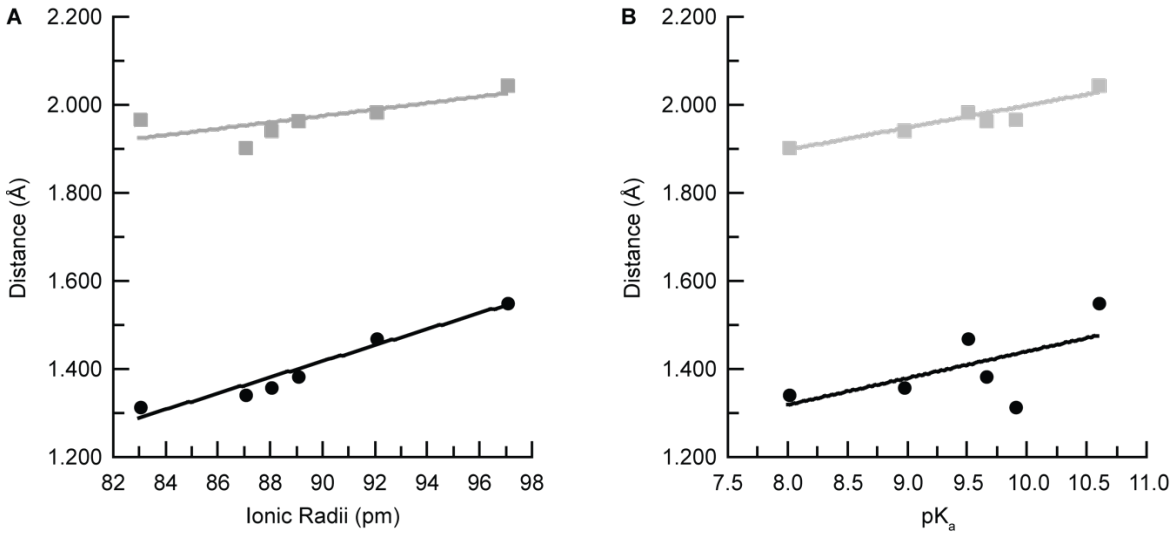

Figure S2. Plots of displacement of the M^{II} ion from the plane formed from the N atoms of the TMTACN ligand (black circles) and M^{II}–O1 bond length (gray squares) versus (**A**) the ionic radii of the M^{II} ions[7] and the (**B**) pK_a values for the $[M^{II}(H_2O)_6]^{2+}$ complexes.[8]

Electron Paramagnetic Resonance Studies.

$[Mn^{II}(OH)Fe^{III}]^+$. No EPR signals were observed from the $[Mn^{II}(OH)Fe^{III}]^+$ complex in parallel- or perpendicular-modes for temperatures < 20 K. For temperatures greater than 20 K, a parallel-mode signal at g = 11 appeared and grew in intensity with increasing temperature (Figure S4). The signal is in the region expected for $S = 2$ signals. The absence of this signal below 20 K and growth at higher temperatures is indicative of an antiferromagnetic exchange coupling between the $S = 5/2$ Fe^{III} and $S = 5/2$ Mn^{II} to give a spin coupled $S_C = 0$ ground state, and $S_C = 2$ as one of the excited state spin manifolds. The temperature dependence of the spectrum was measured. The inset of Figure S4 shows a plot of signal intensity × temperature as a function of temperature where the ordinate axis is proportional to the percentage population of the $S_C = 2$ manifold. This percentage was calculated as a function of temperature based on eq 1 (see main text) and also plotted. The solid-line plot indicated an exchange coupling of $J = +35(3)$ cm^{-1} with the uncertainty indicated by the dashed lines on the figure. The simulation overlaid on the spectra uses eq 1 with the Fe^{III} parameters of $[Zn^{II}(OH)Fe^{III}]^+$ and the Mn^{II} parameters listed in Table 3 (Figure S4). The simulations use a concentration in quantitative agreement with the complex added to solution. The simulation of a previously published EPR spectrum of Mn^{II}TMACN gave $|D| = 0.1$ cm^{-1},[7] which is close to the value derived from the simulations of $[Mn^{II}(OH)Fe^{III}]^+$. The $g = 11$ signal is not from the $S_C = 3$ spin manifold because the simulations for this assignment did not agree with the position or intensity of the data.

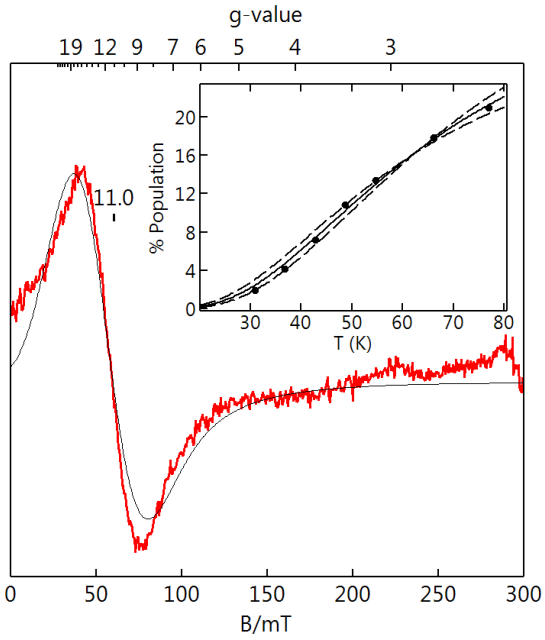

Figure S3. EPR spectra (red) and simulations (black) of $[Mn^{II}(OH)Fe^{III}]^+$ for sample temperature of 66 K. Microwave parameters: 9.334 GHz, 20 mW, $B_1 \parallel B$. See Table 3 in main text for simulation parameters. The inset shows signal intensity × temperature and the corresponding percent population of $S = 2$ for $J = +35(3)$ cm^{-1}. The dashed lines represent the error in J.

$[Fe^{II}(OH)Fe^{III}]^+$. The EPR spectrum of the $[Fe^{II}(OH)Fe^{III}]^+$ complex shows a signal with all g-values < 2 (Figure S5). The low g-values are typical of a mixed-valence species with $S = 2$ Fe^{II} antiferromagnetically exchange coupled to $S = 5/2$ Fe^{III}, which results in the $S_C = 1/2$ spin state lowest in energy. The g-tensor from the $S_C = 1/2$ simulation is **g** = (1.91, 1.68, 1.49). The poor match to data suggests broadening by intermolecular interactions or sample heterogeneity. For temperatures > 20 K, signals from excited spin manifolds are not observed due to signal broadening. The saturation behavior of the ground state $S_C = 1/2$ signal was measured as a function of temperature to determine the exchange coupling constant J. A series of EPR spectra were recorded at multiple microwave powers and multiple temperatures. The power dependence of the signal was fit to determine the power at half-saturation ($P_{1/2}$) at each temperature. The $P_{1/2}$ values as a function of temperature data were then fit using the function, where A = 5.2 μW/K, B = 63 W, and Δ = 56 K (39 cm^{-1}). The first and second terms are due to the direct and Orbach

relaxation processes, respectively, and Δ is the energy of the excited S_C = 3/2 manifold. From the value of Δ, the exchange coupling constant of J = +26(4) cm^{-1} was calculated, with the uncertainty in the value indicated by the dashed lines on the figure.

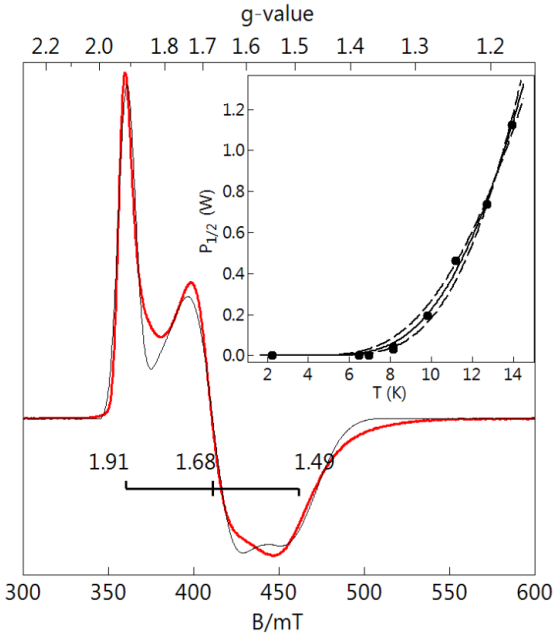

Figure S4. EPR spectra (red) and simulations (black) of $[Fe^{II}(OH)Fe^{III}]^+$ for a sample temperature of 7 K. Microwave parameters: 9.644 GHz, 0.2 mW, $\mathbf{B_1} \perp \mathbf{B}$. For the S_C = 1/2 simulation, **g** = (1.91, 1.68, 1.49). The inset shows the power at half saturation versus temperature, and a fit with for the S_C = 3/2 state at 39 cm^{-1}, see main text for further information.

References

(1) APEX2 Version 2010.3-0, Bruker AXS, Inc.; Madison, WI 2010.
(2) SAINT Version 7.68a, Bruker AXS, Inc.; Madison, WI 2009.
(3) Sheldrick, G. M. SADABS, Version 2008/1, Bruker AXS, Inc.; Madison, WI 2008.
(4) Sheldrick, G. M. SHELXTL, Version 2008/4, Bruker AXS, Inc.; Madison, WI 2008.
(5) International Tables for X-Ray Crystallography 1992, Vol. C., Dordrecht: Kluwer Academic Publishers.
(6) Sano, Y.; Weitz, A. C.; Ziller, J. W.; Hendrich, M. P.; Borovik, A. S. Unsymmetrical Bimetallic Complexes with M^{II}–(μ-OH)–M^{III} Cores ($M^{II}M^{III}$ = $Fe^{II}Fe^{III}$, $Mn^{II}Fe^{III}$, $Mn^{II}Mn^{III}$): Structural, Magnetic, and Redox Properties. *Inorg. Chem.* **2013**, *52*, 10229–10231.
(7) Shannon, R. D. Revised effective ionic radii and systematic studies of interatomic distances in halides and chalcogenides. *Acta Crystallogr. Sect. A* **1976**, *32*, 751–767.
(8) Jackson, V. E.; Felmy, A. R.; Dixon, D. A. Prediction of the pK_a's of Aqueous Metal Ion +2 Complexes. *J. Phys. Chem. A* **2015**, *119*, 2926−2939
(9) Flassbeck, C.; Wieghardt, K.; Bill, E.; Butzlaff, C.; Trautwein, A. X.; Nuber, B.; Weiss, J. Coordination of 4,7-bis(2-hydroxybenzyl)-1-oxa-4,7-diazacyclononane (LH_2) with manganese(II) and -(III) and zinc(II). Crystal structure of $[(LH)_2Zn_2(\mu\text{-}OH)](PF_6)\bullet 0.5CH_3OH$. *Inorg. Chem.* **1992**, *31,* 21–26.